Friction **11**(12): 2204–2220 (2023)
https://doi.org/10.1007/s40544-022-0714-6
ISSN 2223-7690
CN 10-1237/TH
RESEARCH ARTICLE

Fluorinated graphene quantum dots with long-term lubrication for visual drug loading and joint inflammation therapy

Peiwei GONG[1,2,†,*], Changmin QI[1,†], Dandan WANG[1], Mianran CHAO[1], Jianxi LIU[2,*], Meirong CAI[3], Weimin LIU[2,3]

[1] *Key Laboratory of Catalytic Conversion and Clean Energy in Universities of Shandong Province, School of Chemistry and Chemical Engineering, Qufu Normal University, Jining 273165, China*

[2] *State Key Laboratory of Solidification Processing, Center of Advanced Lubrication and Seal Materials, Northwestern Polytechnical University, Xi'an 710072, China*

[3] *State Key Laboratory of Solid Lubrication, Lanzhou Institute of Chemical Physics, Chinese Academy of Sciences, Lanzhou 730000, China.*

Received: 06 May 2022 / Revised: 11 October 2022 / Accepted: 26 October 2022

Abstract: Osteoarthritis (OA) treatment mainly relies on developing new drugs or nanocarriers, while little attention is paid to building novel remedial mode and improving drug loading efficiency. This work reports an integrated nanosystem that not only realizes visual drug loading and release, but also achieves enhanced lubrication and effective joint inflammation therapy based on fluorinated graphene quantum dots (FGQDs). Oxygen introduction promotes FGQDs outstanding water-stability for months, and layered nano-sized structure further guarantees excellent lubricating properties in biomimetic synovial fluid. The special design of chemistry and structure endows FGQDs robust fluorescence in a wide range of pH conditions. Also, the excitation spectrum of FGQDs well overlaps the absorption spectrum of drugs, which further constructs a new concept of internal filtering system to visually monitor drug loading by naked eyes. More importantly, extraordinary long-term lubrication performance is reported, which is the first experimental demonstration of concentration-dependent mutations of coefficient of friction (COF). Cell incubation experiments indicate that drug-loaded FGQDs have good biocompatibility, tracking property of cellular uptake and drug release, which show efficient anti-inflammation potential for H_2O_2-induced chondrocyte degradation by up-regulated cartilage anabolic genes. This study establishes a promising OA treatment strategy that enables to monitor drug loading and release, to enhance long-time lubricating property, and to show effective anti-inflammatory potential for cartilage protection.

Keywords: fluorinated graphene (FG); structure design; lubrication; fluorescence; drug delivery

1 Introduction

Osteoarthritis (OA), known as the "cancer that never dies", is a degenerative joint disease to cause human suffering with a very high incidence in the context of global population aging [1–3]. Insufficient lubrication of synovial fluid irreversibly damages articular cartilage and induces a series of continuous inflammatory reactions of joint capsule, which is closely related to the generation and development of OA [4, 5]. Artificial joint replacement is a termination method for OA treatment, which is prone to many complications and intense discomfort due to severe lack of lubrication [6, 7]. Oral non-steroidal anti-inflammatory drugs with rapid metabolic function cannot effectively treat OA due to the extremely low drug absorption rate of articular cartilage with insufficient blood vessels, and may even infect other organs [8, 9]. Therefore,

† Peiwei GONG and Changmin QI contributed equally to this work.

* Corresponding authors: Peiwei GONG, E-mail: gongpeiwei10@mails.ucas.ac.cn; Jianxi LIU, E-mail: jianxiliu@nwpu.edu.cn

enhancing joint lubrication and simultaneously treating inflammation are of great importance to treat OA more effectively.

As a novel zero-dimensional (0D) carbon nanomaterial, fluorinated graphene quantum dots (FGQDs) have ultra-small size and abundant fluorine groups, which can induce positively biological responsiveness and decreases surface energy [10–12]. Specifically, FGQDs not only inherit outstanding properties of fluorinated graphene (FG), such as high surface area, high mechanical strength, good biocompatibility, and self-lubrication property, but also exhibit greatly improved water-dispersibility and water-stability by introducing oxygen groups [13–15]. And the nearly spherical structure of FGQDs can act like "ball bearings" between friction pairs, which is conducive to rolling friction and further reduces friction [16, 17]. In addition, FGQDs are relatively small and uniform in size, which can easily embed between micro-bumps on the friction interface and accelerates the formation of lubricating films [18]. These superior characteristics make FGQDs hold great promise in biotribology and water-based lubrication. However, as far as we know, FGQDs are rarely investigated for OA treatment, and the corresponding mechanism remains unclear.

On the other hand, most of the present studies on delivering anti-inflammatory drugs are mainly focusing on developing new nanocarriers, while little attention is paid to improving the drug loading efficiency without using large analytical instruments or avoiding complex procedures. The aromatic-conjugated structure and good water solubility guarantee FGQDs as a promising candidate for drug delivery, and many anti-inflammatory drugs can be absorbed by the strong π–π stacking, hydrogen bonding, and hydrophobic interactions among them [19, 20]. Meanwhile, effective design of micro-structure and surface chemistry can endow FGQDs with unique photoluminescence (PL) property [21, 22]. The luminescence behavior of the FGQDs is changed or even quenched after loading with drugs, which can be used to monitor drug loading process visually with naked eyes instead of analytical instruments. Therefore, how to design the structure and chemistry of FGQDs to realize visual drug loading and effective lubrication is highly desirable and practically valuable.

Herein, we developed an FGQDs-based lubricating nanosystem as an integrated model for OA treatment, which realized the visualization of drug loading and release, and effectively delivered anti-inflammatory drugs. Oxygen and fluorine co-existing FGQDs were prepared, and the good water dispersion guaranteed a high drug loading capacity. The FGQDs exhibited bright and robust PL properties independent of pH changes. Moreover, the excitation spectrum of FGQDs was tuned to overlap the absorption spectrum of anti-inflammatory drug of diclofenac sodium (DS), which constructed an internal filtering effect (IFE) system to realize the visual loading of drugs. In addition, toxicity, cell uptake, therapeutic effect of inflammation, and the tribology behavior of drug-loaded FGQDs were systematically investigated in a sodium hyaluronate (NaHA)-based synovial fluid. The integrated system showed visual drug loading convenience with high capacity, excellent antiwear performance with long lubrication life, good biocompatibility, and effective anti-inflammatory effects for cartilage cell protection. An illustration to demonstrate this work is provided in Fig. 1.

2 Experimental

2.1 Raw materials

Raw chemical reagents for synthesizing and characterizing are provided in Section S1.1 in the Electronic Supplementary Material (ESM).

2.2 Preparation of FGQDs

FGQDs were prepared by the top–down method by oxidizing fluorinated graphite (FGi). In brief, FGi was pretreated by liquid intercalation and ultrasonic treatment to prepare a thin layer of FG, and then FG was oxidized and cut by the mixed acid method to obtain FGQDs. The details are explained in Sections S1.2 and S1.3 in the ESM.

2.3 Loading of DS on FGQDs

Ten parts of 0.3 mg/mL FGQDs solution, each 3 mL, were added with 0.09–1.05 mg DS, and stirred at room temperature at 15 rad/s for 24 h without light. FGQDs–DS was prepared by density gradient

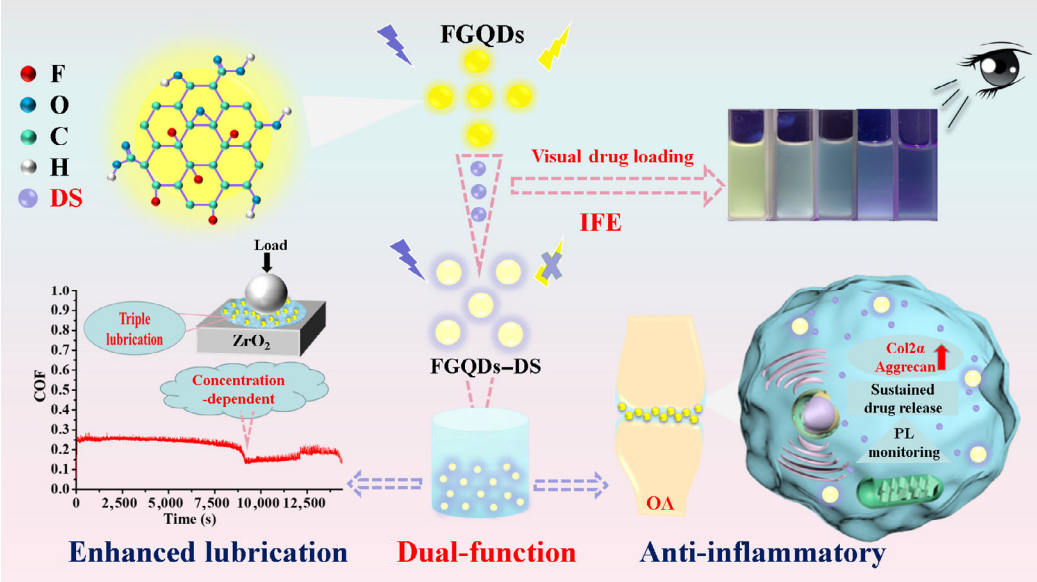

Fig. 1 Illustration for construction of dual-function nanosystem with enhanced lubricating and anti-inflammatory properties.

centrifugation, washing, and vacuum freeze-drying. 3 mL of centrifuged supernatant was taken for the ultraviolet–visible (UV–Vis) test. A series of the standard solution of DS with concentration gradient was accurately prepared, and the related absorbance data were measured. The absorbance–concentration standard curve of DS was plotted with the concentration and corresponding absorbance at 275 nm as horizontal and vertical coordinates, respectively. The concentration of supernatant was determined by searching the standard curve of DS absorbance–concentration drawn above, and the loading rate of DS on FGQDs was calculated by Eq. (1):

$$\text{Loading rate} = \frac{\text{DS}_{\text{initial}} - \text{DS}_{\text{centrifugate}}}{\text{DS}_{\text{initial}}} \times 100\% \quad (1)$$

In addition, FGQDs solution loaded with different amounts of DS was photographed under natural light and UV lamp, and the fluorescence intensity of the solution was measured by the fluorescence spectrophotometer.

2.4 Lubrication performance test

2.4.1 *Preparation of water-based lubricants*

The NaHA aqueous solution of 15 mg/mL was selected as the bionic synovial fluid to prepare water-based lubricants. FGQDs of different qualities were added to the bionic synovial and dispersed evenly by ultrasound to obtain different concentrations of FGQDs–NaHA lubricants in water.

2.4.2 *Tribological experiments*

The tribological properties of the FGQDs-based lubricants were analyzed by a tribometer (TRB3, Anton Paar, the Netherlands) with a ZrO_2 plate (2 cm × 2 cm) and a ball (diameter: 6 mm) in a reciprocating mode. The test conditions are reciprocating distance: 2 mm, frequency: 1–5 Hz, load: 1–5 N, test time: 30, 180, and 240 min, and temperature: 25 °C. The coefficient of friction (COF) was recorded automatically by a computer system connected to the tribometer. After the test, the contour, depth, and width were determined by the three-dimensional (3D) profilometer, and the wear volume was calculated by the calculation equation of the cylinder. The scanning electron microscopy (SEM; Sigma500, Zeiss, Germany) and energy dispersive spectroscopy (EDS) elemental mappings were used to analyze the characteristics of wear surface. All long-time lubrication tests were under optimal test conditions.

2.5 Cytotoxicity study

The toxicity of FGQDs toward MC3T3-E1 osteoblast cells was determined by methyl thiazolyl tetrazolium (MTT) assay. FGQDs with different concentration

gradients were added to the cell culture medium and incubated with cells for 24, 48, and 72 h, and the absorbance of the solution was measured with a microplate reader. The specific steps are in Section S1.4 in the ESM.

2.6 Laser confocal scanning microscopy (LCSM) experiment

To observe drug release in osteoblasts more clearly, rhodamine B (RhB) with strong fluorescence was used instead of DS, and the LCSM with the dual-channel function was used for fluorescence imaging experiments. The details are shown in Section S1.5 in the ESM.

2.7 Quantitative real-time (qRT)-polymerase chain reaction (PCR) analysis

To further investigate the effect of FGQDs–DS on the degradation of inflammation-induced chondrocytes, chondrocytes were incubated into a six-hole plate at a density of 8×10^5 cells per hole and treated with 15 mU H_2O_2 first. They were co-cultured with FGQDs–DS, FGQDs, and DS for 24 h. The details of the experiment are explained in Section S1.6 in the ESM.

2.8 Characterization and performance test

Details of the instruments used for characterization and performance tests in this work are provided in Section S1.7 in the ESM.

3 Results and discussion

3.1 Morphologies, structures, and chemical compositions of FGQDs

The morphologies of the prepared FGQDs were determined by the transmission electron microscopy (TEM). FGQDs were spot-shaped and uniformly distributed in size (Fig. 2(a) and Fig. S1 in the ESM). The high-resolution transmission electron microscopy (HRTEM) image in the inset showed an average lattice spacing of 0.21 nm for the FGQDs, which belonged to the in-plane (100) crystal face of graphene with a high crystallinity structure [23]. Statistical analysis results showed that the particle sizes of FGQDs were principally distributed between 2.5 and 4 nm (about 77%), and such a small size was conducive to promoting intracellular phagocytosis [24]. The outstanding mono-dispersity and dimensional uniformity of FGQDs

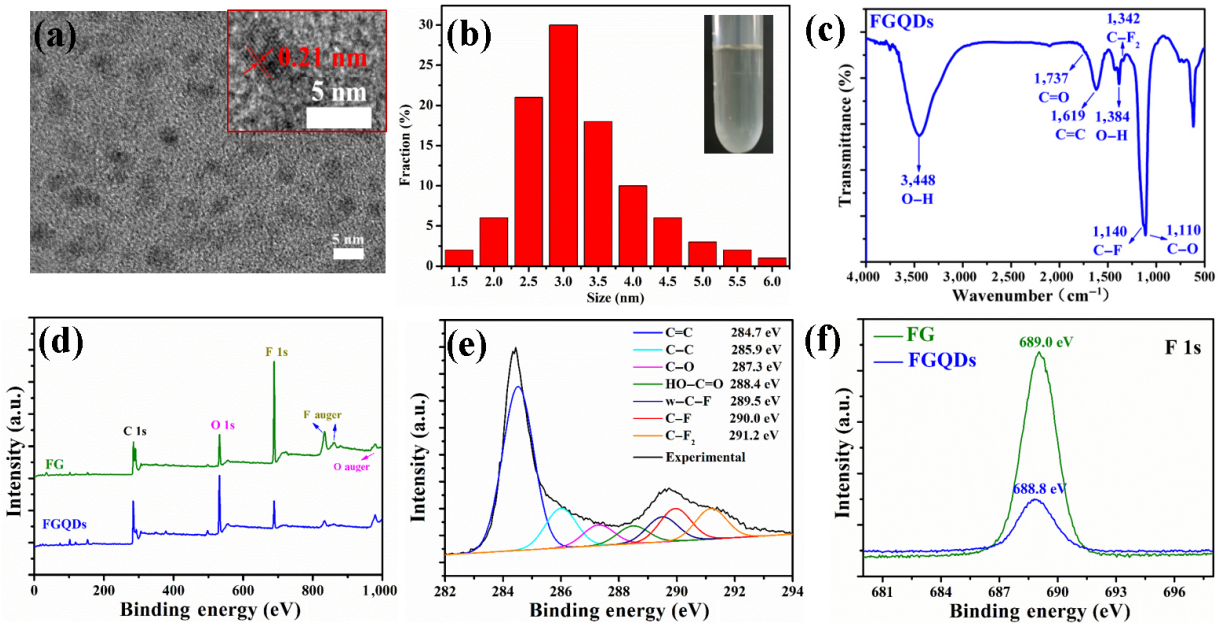

Fig. 2 Characterization of FGQDs and FG. (a) TEM and HRTEM images of FGQDs; (b) size distribution histogram of FGQDs (the inset shows the solution dispersion and stability of FGQDs in water); (c) Fourier transform infrared (FTIR) spectrum of FGQDs; (d) X-ray photoelectron spectroscopy (XPS) survey spectra of FG and FGQDs; and (e) high-resolution C 1s spectra of FGQDs and (f) high-resolution F 1s spectra of FG and FGQDs.

can be attributed to the fact that FGQDs were synthesized in a uniformly heated mixed acid solution, and the homogenized oxidized cutting environment created favorable conditions for the formation of FGQDs.

In addition, the FTIR spectrum was performed on the FGQDs to determine their functional groups. As shown in Fig. 2(c), the peaks at 1,342 and 1,140 cm^{-1} were derived from the stretching vibration of C–F_2 and C–F bonds, respectively [21, 25]. All the above suggested the stable retention of C–F bonds on the carbon skeleton. Both the locations of 1,737 cm^{-1} (C=O stretching vibration) and 1,110 cm^{-1} (C–O–C antisymmetric stretching vibration) confirmed the introduction of oxygen-containing functional groups [26]. Meanwhile, the peak center of wide absorption at 3,448 cm^{-1} (O–H stretching vibration) and 1,384 cm^{-1} (O–H bending vibration) indicated that the surface of FGQDs contained O–H groups [27]. The existence of the aforementioned C=O, O–H, and other hydrophilic groups ensured that FGQDs had good dispersion and water solubility in water, which were also verified by its light yellow, uniform, and transparent state (the inset of Fig. 2(b)).

The chemical compositions and functional group information of FGQDs were further confirmed by the X-ray photoelectron spectroscopy (XPS). Figure 2(d) only shows the characteristic peaks of carbon (C), oxygen (O), and fluorine (F), suggesting that the sample was relatively pure. Notably, compared with that of FG, the content of oxygen in FGQDs increased, while the content of fluorine decreased significantly, which indicated that the transformation from FG to FGQDs introduced hydrophilic oxygen groups. In addition, oxygen-containing groups of C–O (287.3 eV), HO–C=O (288.4 eV), and fluoride groups of weak C–F (w-C–F; 289.5 eV), C–F (290.0 eV), and C–F_2 (291.2 eV) were detected in the C 1s spectrum (Fig. 2(e)) [28]. Combined with that of FG (Fig. 2(f)), the F 1s spectrum peak value of FGQDs located at about 688.8 eV was lower than that of FG located at 689.0 eV, indicating some decrease of fluorine contents during the synthesis process [29]. The results of the XPS were consistent with the FTIR results, both of which proved the existence of hydrophobic fluorine and hydrophilic oxygen groups on the carbon structure, which made FGQDs possess a special driving force for drug loading in water-based solution.

3.2 PL performance characterization of FGQDs

The surface doping structure and small size characteristics endow FGQDs with excellent PL performance. As shown in Fig. 3(a), by special design of reaction conditions, the prepared FGQDs generated an intense yellow emission centered at 531 nm under the excitation of 300 nm. A strong and broad peak centered at 300 nm appeared in the excitation spectrum monitored at the PL of 531 nm. A weaker shoulder peak at 470 nm along with the main excitation was attributed to the combined effect of FGQDs eigenstate and defect state emission [21]. Especially, FGQDs emitted bright yellow fluorescence (the inset of Fig. 3(a)), while the emission wavelengths of most carbon-based quantum dots were mainly concentrated

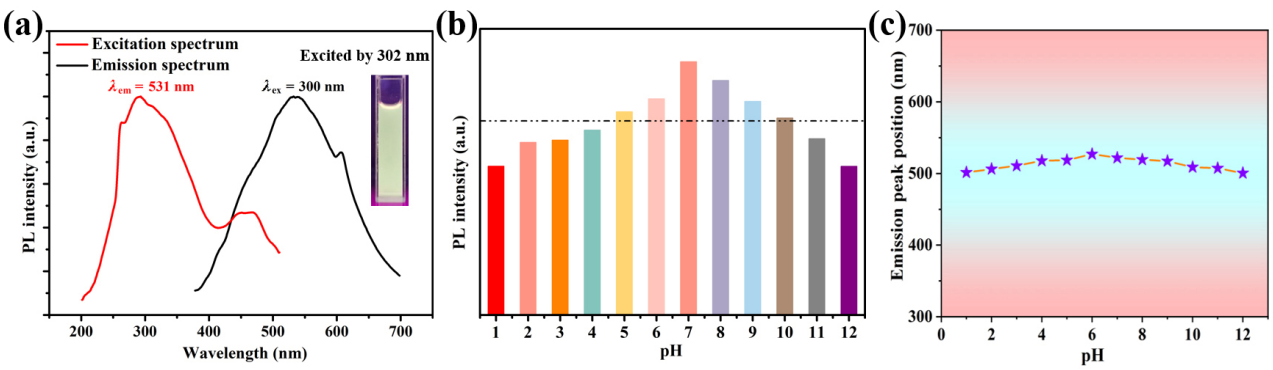

Fig. 3 PL performance of FGQDs dispersed in water at room temperature. (a) Emission and excitation spectra of FGQDs (the inset shows the luminescent image being excited by a UV beam); pH effects on (b) PL intensity and (c) emission peak position of the FGQDs at the highest intensity (the dotted line in (b) is the average intensity). Note: λ_{em} and λ_{ex} in (a) are the emission wavelength and excited wavelength, respectively.

in the blue region, which often interfered with the biological endogenous blue fluorescence imaging [18]. Thus, the unique yellow emission of the FGQDs can avoid the interference problem in biological imaging.

Figure 3(b) shows the PL intensity and emission peak values of the FGQDs under different acid–base environments. We found that the PL intensity of FGQDs maintained a high value even when the pH was changed from 1.0 to 12.0, indicating that the fluorescence of FGQDs did not quench even in strong acid and strong base environments. In addition, FGQDs emission peaks were not significantly affected by the wide-range pH change. The above results indicated that FGQDs maintained strong and stable PL performance in different acid and alkaline environments, making FGQDs different from other graphene and carbon-based quantum dot materials that usually exhibited fluorescence quenching effect under acidic conditions. The unique PL behavior of FGQDs benefited from the presence of fluorine atoms, which acted as the role of passivation, and affected the charge distribution and surface energy of the carbon skeleton [30]. These results suggested that the powerful pH resistance property of FGQDs had higher potential in the field of bio-imaging with various acid–base environments.

3.3 Drug loading performance

Due to the high aromatic specific surface area and good solubility and dispersion in a variety of media (Fig. 4(d)), FGQDs are good candidates for loading aromatic drug molecules [19]. DS is a potent, non-selective aromatic anti-inflammatory drug that can be delivered into cells to relieve pain from diseases such as OA [31]. FGQDs are expected to load DS by strong π–π stacking, hydrogen bonding, and hydrophobic–hydrophobic interactions [20]. To verify this conjecture, different doses of DS were added to the FGQDs solution. As shown in Fig. 4(a), the PL intensity of FGQDs decreased gradually with continuous addition of DS, which was attributed to the IFE caused by the large degree of overlap between the absorption spectrum of DS and the excitation spectrum of FGQDs (Fig. S2 in the ESM) [32–34]. The DS that absorbed on FGQDs acted as a mask, which generated continuous decrease of PL intensity.

When the FGQDs loaded with different doses of DS were exposed to UV and natural light, visual monitor of drug loading was achieved (Fig. 4(b)). As increasing of the DS loading, the color of the solution under the natural light tended to gradually darken.

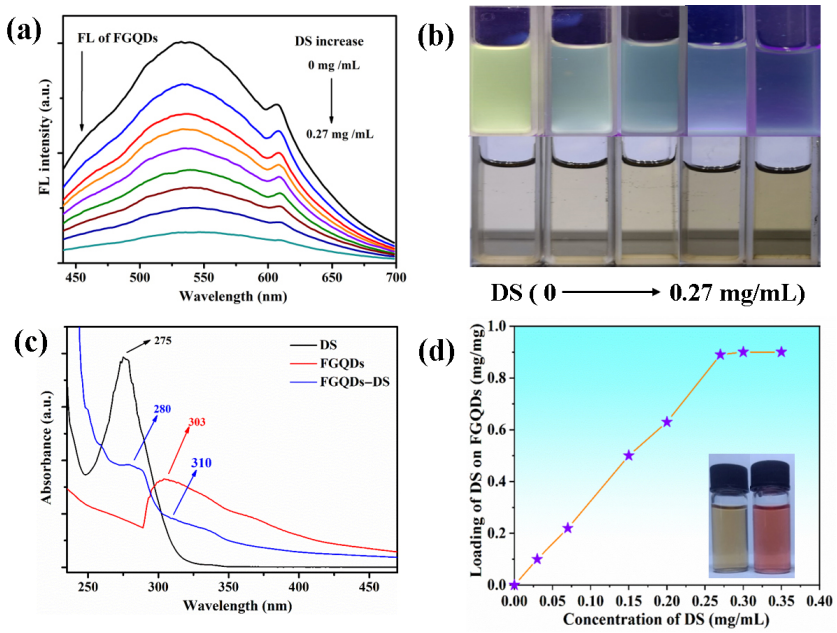

Fig. 4 Visualization of drug loading. (a) Fluorescence (FL) intensity changes of FGQDs after being loaded with different amounts of DS; (b) color changes of FGQDs solution under UV light and natural light with the concentration of DS increasing from 0 to 0.27 mg/mL; (c) UV–Vis spectroscopy for the samples; and (d) loading curve of DS on FGQDs (the inset shows the solution stability of FGQDs–DS in phosphate buffered saline (PBS) and cell culture).

When the corresponding solution were placed under the UV lamp, obvious color gradient were clearly observed: The bright yellow fluorescence (DS concentration: 0 mg/mL) gradually turned into dark green, and finally presented very weak blue–purple fluorescence. Due to the IFE, the yellow fluorescence of FGQDs was almost quenched [33, 35]. When the concentration of DS increased to 0.27 mg/mL, only the faint blue–violet fluorescence of DS loaded by FGQDs was observed under the UV lamp.

Based on the IFE, degree of drug loading on the FGQDs–DS system can be effectively judged by observing the color changes with naked eye, which suggested that FGQDs could be used as a special and visual sensor to monitor drug loading process, thus avoiding the use of additional instruments such as the UV–Vis spectrophotometer and greatly improving efficiency. In addition, the effective drug loading results were further confirmed by the UV–Vis test. As shown in Fig. 4(c), the peak at 280 nm and the broad peak at 310 nm were mainly detected in the sample after loading, which came from the characteristic peak of 275 nm for DS and the characteristic peak of 303 nm for FGQDs. It is worth noting that the overall absorption peak of FGQD–DS was redshifted to a certain extent, which was mainly attributed to the increase of π–π conjugated system [36], which further confirmed successful drug loading. It can be seen that the maximum drug loading rate of FGQDs was 0.91 mg/mg (Fig. 4(d)), which certified the outstanding performance of FGQDs in the reported drug-loaded quantum dots. As far as we know, this is the highest DS loading capacity for carbon materials. These results indicated that the FGQDs held great promise as nanocarrier for sensing visual drug loading.

3.4 Tribological test

The uniform size and good hydrophilicity make FGQDs have a broad application prospect as a lubrication additive in aqueous environment. Due to its high hardness, abrasion resistance, and corrosion resistance, ZrO_2 ceramic can be used as a friction pair of ball head for artificial joint replacement [37, 38]. Therefore, it is feasible to use ZrO_2 as a friction pair material to evaluate the tribological performance of OA. In order to simulate the friction environment of joint more realistically, a series of FGQD–NaHA bionic synovial fluids were prepared using ZrO_2 plate and ball as friction pairs to evaluate the tribological properties of FGQDs. The test conditions such as frequencies, loads, and concentrations of FGQDs were screened and optimized first. As shown in Fig. 5(a), the COF tended to decrease with the increasing reciprocating frequency at 5 N, although the difference between 3 and 5 Hz was not significant at 5 mg/mL. In addition, by fixing reciprocating frequency at 5 Hz to perform the COF measurement under different loads, we can clearly see in Fig. 5(b) that the COF of different concentrations of FGQDs all showed a trend of decrease with the increase of load, which indicated that FGQDs showed better lubrication performance under relatively high loads. According to Figs. 5(a) and 5(b), it can be seen that 5 N and 5 Hz were the best test conditions for this work. It is worth noting that when the concentration of FGQDs was 3 mg/mL, the COF was relatively lower. This may be caused by the following reasons: At the initial stage of friction, the hydrophilic ZrO_2 adsorbed water molecules and FGQDs stably dispersed in aqueous solution together to the surface of the friction pairs through strong hydrogen bonding. As a result, FGQDs acted as an effective protective shell in the contact area of the friction pairs, avoiding direct contact of the friction pairs. Ultra-small and nearly spherical FGQDs can roll between friction pairs, acting like "ball bearings", changing the form of friction from sliding friction to rolling friction, which is the main factor for the lubrication in the beginning of friction [12, 18]. Low concentrations of the FGQDs led to higher COFs and had no efficient lubrication. Similarly, when the concentration of FGQDs was too high to become an "obstacle", which made it difficult to slip between FGQDs, and thus the COF increased.

To further evaluate the lubrication performance of FGQDs, we carried out several parallel experiments under the best test conditions. As shown in Fig. 5(c), with the COF of H_2O as the control group, it was found that the COF of FGQD–NaHA solution decreased by 60.72%, and that of FGQD–H_2O solution without NaHA reduced by 53.33%, while the COF of NaHA solution only decreased by 16.67%. It can be seen that FGQDs effectively reduced the COF. Meanwhile, it can be seen in Fig. 5(d) that the COFs of H_2O and

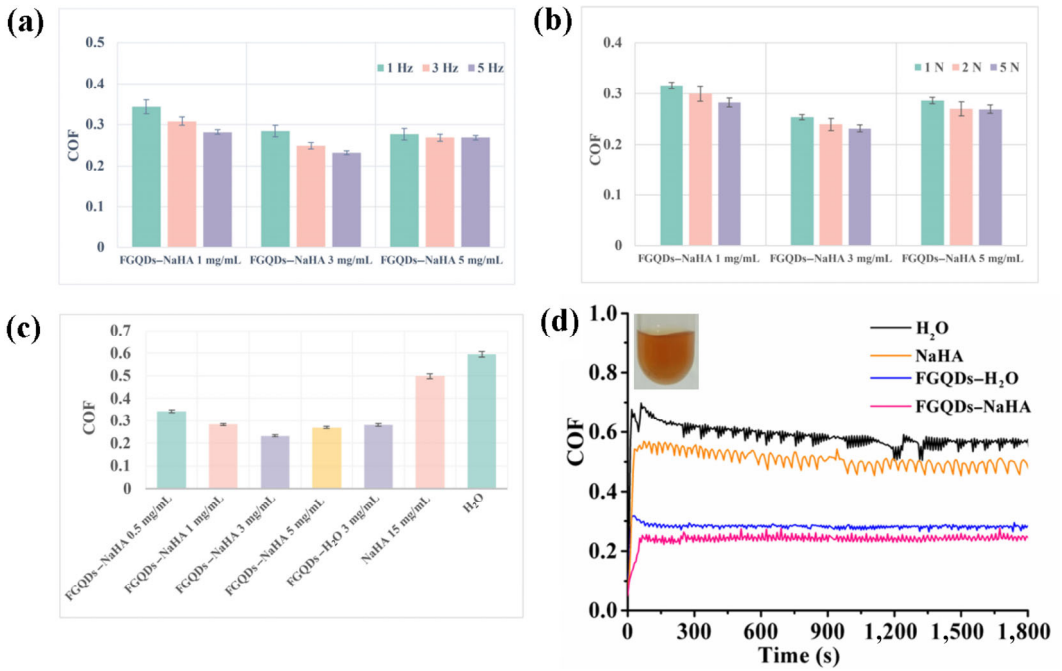

Fig. 5 Tribological test of FGQDs in aqueous dispersion for 30 min. Histograms of COF for FGQDs at (a) different frequencies (load: 5 N, reciprocating distance: 2 mm, and temperature: 25 °C) and (b) different loads (frequency: 5 Hz, reciprocating distance: 2 mm, and temperature: 25 °C); (c) comparison of COFs for H_2O, NaHA, FGQDs–H_2O, and different concentrations of FGQDs–NaHA (frequency: 5 Hz, load: 5 N, reciprocating distance: 2 mm, and temperature: 25 °C); and (d) COF curves for H_2O, NaHA, 3 mg/mL FGQDs–H_2O, and FGQDs–NaHA (frequency: 5 Hz, load: 5 N, reciprocating distance: 2 mm, and temperature: 25 °C; the inset shows the solution stability of FGQDs–NaHA after one month).

NaHA are high, and the curve is unstable, while the presence of FGQDs significantly reduced the COF and made the curve smooth and stable, both for FGQDs–H_2O and FGQDs–NaHA. The stability of curve is attributed to the ultra-small size and uniformity of FGQDs, which make FGQDs strong in embedding between micro-bumps at the friction interface. The illustration (Fig. 5(d)) shows that the color of FGQDs–NaHA solution was uniform and clear. Thanks to the presence of hydrophilic functional groups, it can maintain high dispersibility for more than one month at room temperature, which is very significant for water-based lubrication. These results indicated that FGQDs significantly reduced the COF under high loads and relatively low concentrations, which were expected to be an excellent antifriction system as joint synovial fluid additives.

3.5 Wear surface profile analysis

The antiwear property of lubricant is also crucial for their practical application in water-based environments. The antiwear performance of different lubricants was studied and compared by profile of wear trajectory analyses. Figure 6 shows the two-dimensional (2D) and 3D profiles and corresponding cross-sectional profiles of wear tracks on the wear surfaces gained by H_2O, NaHA–H_2O and 5 mg/mL FGQDs–NaHA, and 3 mg/mL FGQDs–NaHA for 3 h. By adding FGQDs in NaHA, the wear depth became much shallower than those of H_2O and NaHA. Notable, the wear depth lubricated with 3 mg/mL FGQDs–NaHA additive was simpler and lighter than that of the 5 mg/mL FGQDs–NaHA. The wear volume of 3 mg/mL FGQDs–NaHA additive decreased by 70.09% compared with that of H_2O. As shown in Figs. 7(a) and 7(b), the wear volumes of H_2O, NaHA–H_2O, 5 mg/mL FGQDs–NaHA, and 3 mg/mL FGQDs–NaHA were 3,925, 1,591, 1,300, and 1,174 μm^3, respectively. The wear volume of H_2O lubrication was very large, and the friction surface had serious wear tracks. These results suggested that FGQDs could further improve the antiwear property of H_2O and NaHA due to the combination of the filling effect of ultra-small FGQDs and the formation of FGQDs lubrication film on the

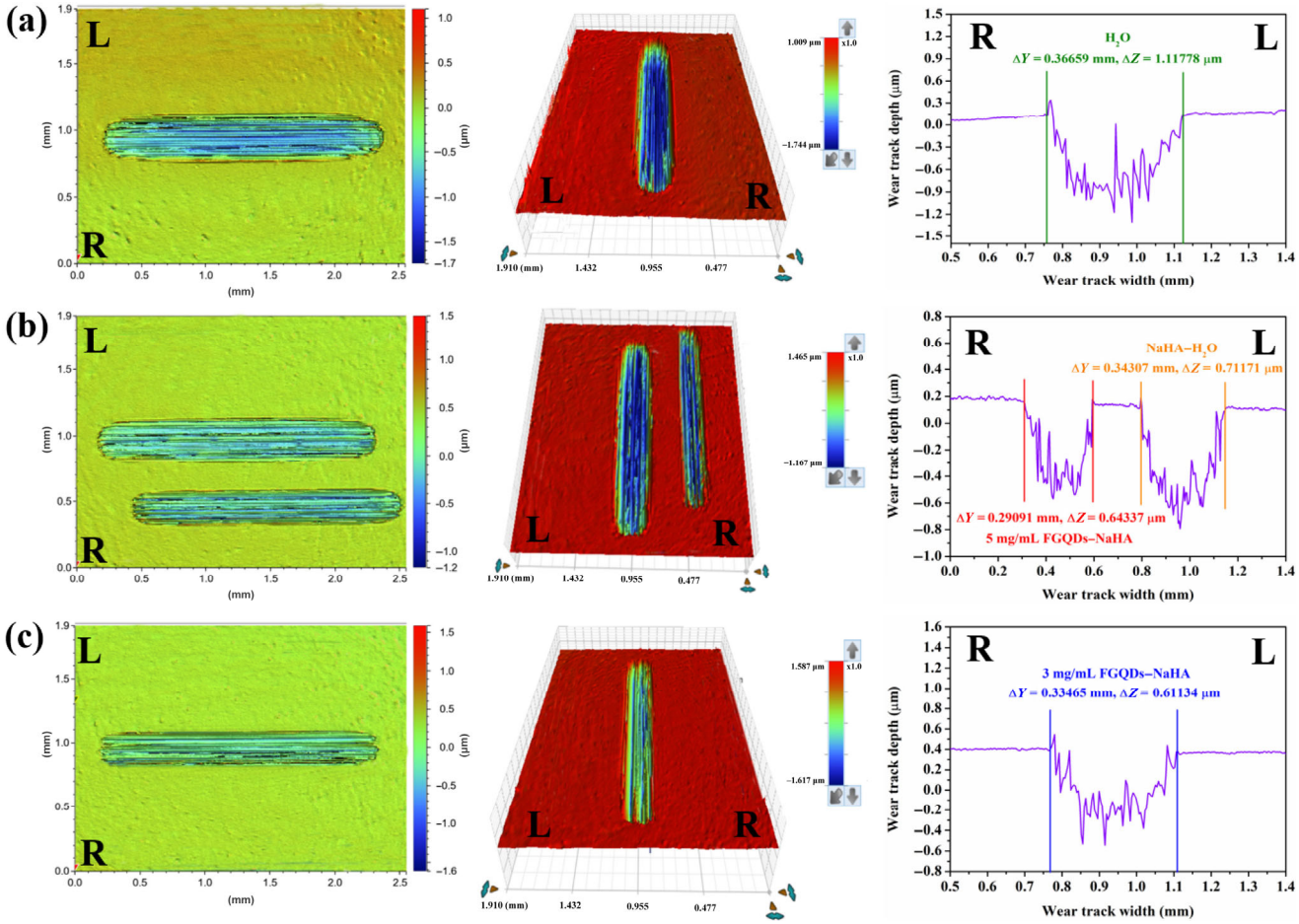

Fig. 6 2D and 3D profiles and corresponding cross-sectional profiles of wear tracks on the wear surfaces gained by (a) H_2O, (b) NaHA–H_2O and 5 mg/mL FGQDs–NaHA, and (c) 3 mg/mL FGQDs–NaHA for 3 h. Note: Land R represent left and right, respectively.

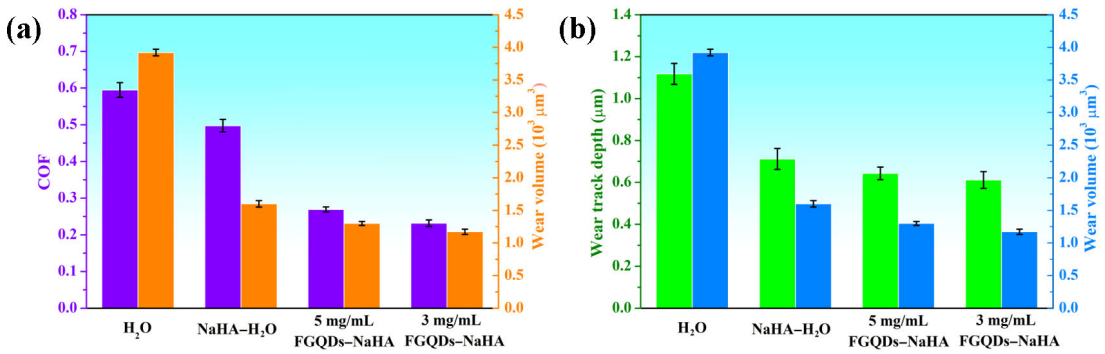

Fig. 7 (a) COFs and wear volumes and (b) wear track depths and wear volumes obtained by H_2O, NaHA–H_2O, 5 mg/mL FGQDs–NaHA, and 3 mg/mL FGQDs–NaHA lubricants for 3 h.

friction surface. In particular, the wear depth lubricated with 3 mg/mL FGQDs–NaHA additive was simpler and lighter than that of the 5 mg/mL FGQDs–NaHA. This further confirmed that excessive amounts of FGQDs were easily aggregated and were not beneficial to friction reduction. The change in wear volume was consistent with the trend reflected by the COF (Fig. 7(a)). The results showed that FGQDs possessed better antifriction and antiwear properties at a lower concentration.

3.6 Long-term lubrication and comprehensive analyses of wear surfaces

To further evaluate the service life of lubrications based on FGQDs, the COF curves for 3 h were monitored under optimal test conditions (Fig. 8(a)). The COF of H_2O was the largest; although the addition of NaHA slightly reduced the COF, the lubrication effect was not obvious. The COFs of both H_2O and NaHA suddenly increased at the later stage of friction and reached the high value finally, which were close to the COF of bare friction pairs, indicating that H_2O and NaHA did not maintain good lubrication performance for a long time, and lubrication failure occurred. The introduction of FGQDs resulted in a significant reduction in COF. It was noted that after 8,980 s, not only did no lubrication failure occur, but COF suddenly decreased and remained stable for a period of time, indicating that FGQDs showed fine and special lubrication performance. This mutation phenomenon drove us to conduct subsequent more detailed friction tests to study the relationship between the concentration of FGQDs and COF (Figs. 8(a), 8(b), and 8(d)). It was found that the higher the concentration of FGQDs, the earlier the mutation appeared. The COF curves of FGQDs at different concentrations showed a similar trend, with a slight decrease in COF in the time before mutation. COF mutations may be caused by the formation of a lubricating transfer film in the contact area. In a certain range of FGQDs concentrations, the more FGQDs existed, the earlier lubrication film formed; and accordingly, the decrease of COF was obtained. Thus, higher concentration of FGQDs contributed to the quick formation of lubrication film, while the best lubrication conditions were only obtained with suitable concentration of FGQDs.

The SEM and EDS tests of wear tracks further revealed the characteristics of wear surface and the role of FGQDs in lubrication. The SEM data (Fig. 8(e)) indicate that FGQDs showed repair effect by filling deep scratches, which directly explained the superior antifriction and antiwear properties. In addition, the wear surface of 5 mg/mL was relatively rough, which was very consistent with the 3D profile data (Section 3.5). The EDS analysis further confirmed the formation of FGQDs-based transfer film on the friction surface of ZrO_2 plate. As shown in Fig. 8(f), the relative contents of the mutated elements were not significantly different, which was due to the stable generation of transfer film, and indicated that FGQDs and ZrO_2 were relatively stable without significant chemical reactions, which also indicated the potential application of FGQDs in joint synovial fluid additives. In addition, The EDS analysis was performed on the wear surfaces before and after mutation (Table S1 in the ESM). Compared to the situation before mutation, the relative content of FGQDs-related elements on the wear surfaces decreased after mutation, which was caused by the fact that some samples were pushed out of the contact interface during this long period of friction journey.

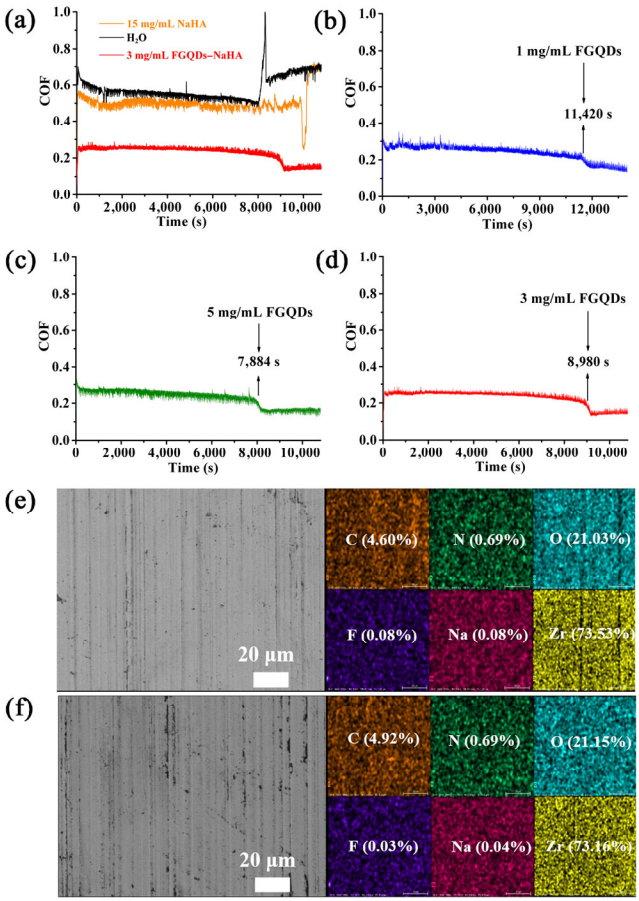

Fig. 8 Long-term lubrication performance of FGQDs under optimal test conditions. (a) Curves of COF for H_2O, NaHA, and FGQDs–NaHA for 3 h (frequency: 5 Hz, load: 5 N, reciprocating distance: 2 mm, and temperature: 25 °C); (b–d) curves of COF for FGQDs–NaHA at different FGQDs concentrations. SEM images and EDS elemental mappings of wear surfaces on ZrO_2 plate lubricated by (e) 3 mg/mL and (f) 5 mg/mL FGQDs–NaHA for 3 h.

3.7 Lubrication mechanism

To further verify the lubrication mechanism of FGQDs, 3 and 10 mg/mL FGQDs–NaHA were tested for a long time of 4 h (Figs. 9(a) and 9(b), respectively). During the running-in period, FGQDs evenly dispersed in water and were adsorbed between the friction surfaces by hydrophilic ZrO_2 via hydrogen bonds. The COF decreased slowly and steadily before mutation due to the co-lubrication caused by rolling and filling effect between ultra-small nanosheets of FGQDs [39, 40]. The curve showed that the more FGQDs were added, the earlier mutation appeared, which was consistent with the conclusion obtained in Section 3.6. The mutation of COF was attributed to the formation of low friction transfer film between the contact surfaces of friction pairs [41, 42]. The higher the concentration of FGQDs, the shorter the running-in period and the easier the formation of uniform transfer film, which was consistent with the prediction made in Section 3.6. Interestingly, with the advance of friction time, the transfer film gradually broke under high shear stress and high frequency contact, and the COF gradually rose to the value that before the mutation, which directly explained the reason for the sharp increase of COF within 13,200–18,000 s. Obviously, the transfer film generated at high FGQDs concentrations was less likely to rupture and provided more effective lubrication for longer periods of time.

Based on the above results, we believe that FGQDs-based additives can greatly improve the tribological properties of water-based lubrication, which can be attributed to the triple lubrication of FGQDs, including rolling effect, filling effect, and formation of uniform transfer film. FGQDs are expected to be widely used in joint synovial fluid as a high-performance water-based lubricant additive.

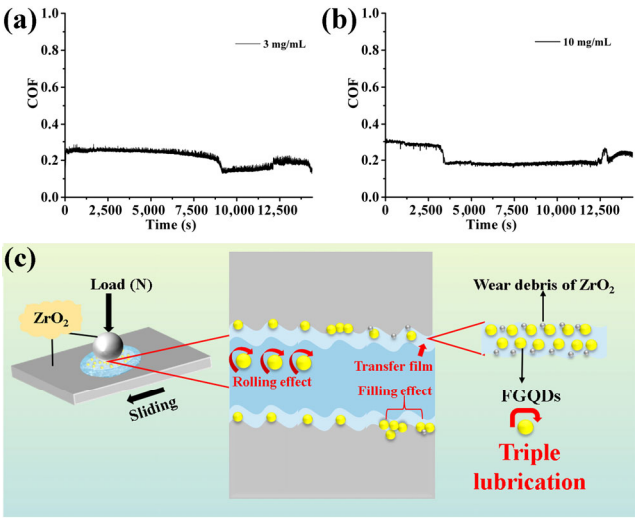

Fig. 9 COF curves for (a) 3 mg/mL and (b) 10 mg/mL FGQDs–NaHA for a long time of 4 h (frequency: 5 Hz, load: 5 N, reciprocating distance: 2 mm, and temperature: 25 °C). (c) Proposed lubrication mechanism.

3.8 Cytotoxicity of FGQDs

To further explore the possibility of application for FGQDs in the biomedical field, MC3T3-E1 osteoblast cells were used as a model to study the potential toxicity through MTT experiments. The cells were co-incubated with different concentrations of FGQDs (0, 10, 20, 50, 100, and 150 μg/mL), and the cell activity was evaluated after 24, 48, and 72 h. As shown in Fig. 10, even when the concentration of FGQDs was as high as 150 μg/mL, the cell viability still exceeded 90% after 24 h incubation, which indicated that FGQDs had no obvious toxicity to living cells. It is noteworthy that the cell viability increased gradually with the extension of co-culture time, which was attributed to the extremely small size, high oxygen content, and low damage to cell membranes of FGQDs. These results

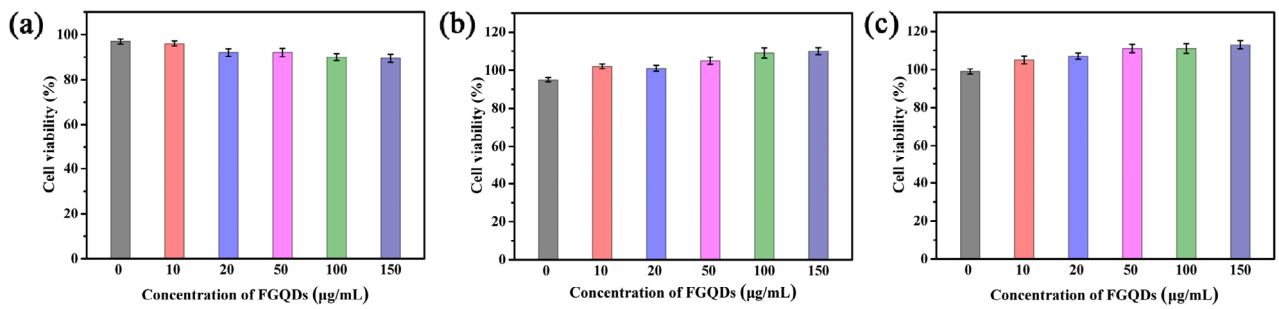

Fig. 10 Toxicity of FGQDs toward MC3T3-E1 osteoblast cells after (a) 24, (b) 48, and (c) 72 h.

suggested that MC3T3-E1 osteoblast cells were tolerant to high-concentration and long-time incubation of FGQDs, which possessed excellent biocompatibility and had great potential in drug loading and delivery applications.

3.9 Behavioral tracking of cellular uptake and drug release

Using FGQDs with low cytotoxicity and excellent fluorescence properties can directly monitor cell uptake behavior through the LCSM, and drug release could be tracked by fluorescence colocalization imaging of both RhB and FGQDs. Cells were co-cultured with FGQDs–RhB for different time. As shown in Fig. 11(a), both yellow (FGQDs) and red (RhB) fluorescence appeared in the cytoplasm of osteoblasts after 1 h, suggesting that FGQDs could enter osteoblasts through endocytosis. In addition, the merged image (the rightmost of Fig. 11(a)) proves that a small amount of RhB was released from the carrier. With the prolongation of co-culture time, the merged image (the rightmost of Fig. 11(b)) shows significantly enhanced red fluorescence after 4 h, indicating that more RhB were released from FGQDs at this time. The results suggested that osteoblasts easily took up FGQDs and released drugs, indicating that FGQDs could simultaneously serve as a bioimaging medium and a good drug delivery tool.

3.10 Protection of FGQD–DS against chondrocyte degradation

The pathogenesis of OA is related to oxidative stress, excessive mechanical loading stress, inflammatory factors, and other factors, which may lead to the degradation of chondrocytes and promote the production of proteolytic enzymes, and the appearances of these symptoms are fairly significant features of OA [31, 43, 44]. In this study, we used H_2O_2-treated chondrocytes as a model to simulate the oxidative stress environment during the pathogenesis of OA [45]. Col2α and aggrecan are vital components of cartilage regeneration, and detecting mRNA expression levels of anabolic factors (Col2α and aggrecan) can analyze the degradation of chondrocytes [46]. After H_2O_2 was added, the mRNA expressions of Col2α and aggrecan decreased gradually with the extension of induction time, and the decreasing amplitude was similar (Figs. 12(a) and 12(b)). It is noteworthy that after 12 and 24 h, the mRNA expressions of aggrecan decrease to about 1/4 and 1/6 of the initial value (0 h), respectively (Fig. 12(b)), indicating a rapid rate of inflammation induction in the first 12 h and demonstrating that the treatment of H_2O_2 had effectively induced inflammation in chondrocytes.

To investigate whether FGQDs–DS had a protective effect on chondrocyte degradation induced by oxidative stress, we added FGQDs, FGQDs–DS, and DS into chondrocytes and treated them for 24 h. As shown in Figs. 12(c) and 12(d), the mRNA expressions in the FGQDs group were very low and close to those of the blank group (chondrocytes treated with H_2O_2 only). On the contrary, the mRNA expression levels of Col2α and aggrecan increased significantly after treatment of FGQDs–DS or DS and reached more than 70% of the

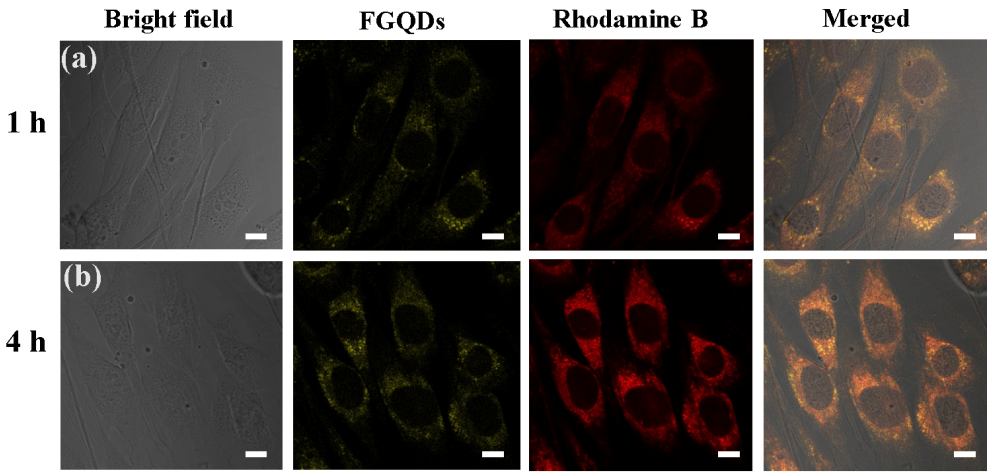

Fig. 11 LCSM images of MC3T3-E1 osteoblast cells treated with FGQDs–RhB for (a) 1 h and (b) 4 h. Scale bar is 10 μm.

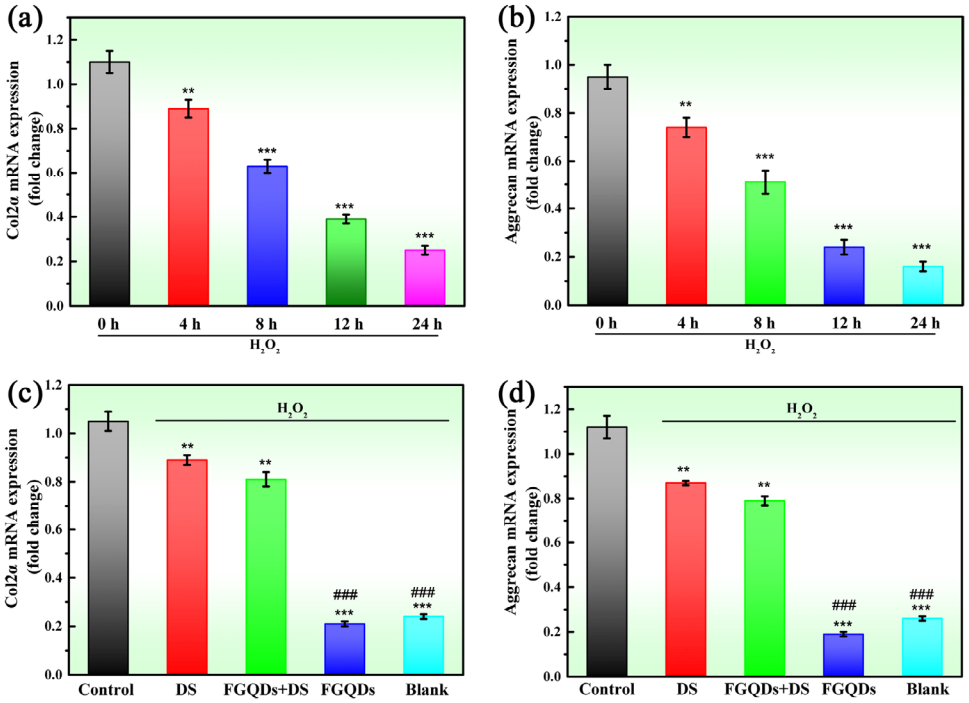

Fig. 12 mRNA expressions of (a) Col2α and (b) aggrecan detected by the qRT-PCR analysis in chondrocytes treated with 15 mU H_2O_2 at different time. Note: $n = 3$, $^{*}P < 0.05$, $^{**}P < 0.01$, and $^{***}P < 0.001$, compared with the control group (0 h). (c, d) mRNA expressions of (c) Col2α and (d) aggrecan exhibited in chondrocytes after treatment of 15 mU H_2O_2 and incubated with FGQDs, FGQDs–DS, and DS for 24 h. Note: $n = 3$, $^{**}P < 0.01$, and $^{***}P < 0.001$, compared with the control group; $^{\#\#\#}P < 0.001$, compared with FGQDs–DS.

control group (normal chondrocytes), which suggested that FGQDs–DS had protective potential against the degradation of inflammatory chondrocytes induced by oxidative stress, and the result also reflected that FGQDs–DS had an effective anti-inflammatory effect. In a word, the above results suggested that drug-delivered FGQDs–DS system can achieve effective anti-inflammatory potential for cartilage protection, thereby inhibiting the development of OA.

4 Conclusions

In summary, we reported a new concept of integrated therapy model that effectively combined with enhanced lubrication and local anti-inflammatory drug intervention to treat OA. Well-designed nanostructure and introduction of oxygen endowed FGQDs with long-time stability in water and stable PL emission in both acid and alkali conditions. The excitation spectrum was adjusted to overlap the absorption peak of DS, and this finally created an effective IFE system to realize visual monitor drug loading and release process. Ultra-small size and nearly spherical rolling effect made FGQDs show excellent antifriction and antiwear property. The COF and wear volume reduced by 60.72% and 70.09%, respectively. Especially, distinguished long-term lubrication was readily obtained, and an emerging concentration-dependent mutations of COF was reported for the first time. Cell studies revealed that drug-loaded FGQDs had good biocompatibility and tracking property of cellular uptake and drug release, and provided protective anti-inflammatory potential for H_2O_2-induced chondrocyte degradation by up-regulated cartilage anabolic genes of Col2α and aggrecan. The newly developed system can realize the visual monitoring of anti-inflammatory drug loading and releasing and show extraordinary lubricating properties and effective anti-inflammatory potential for cartilage protection, which provide a new idea for synergistic OA therapy.

Acknowledgements

This research was supported by the National Natural Science Foundation of China (51905304, 52275202,

and 21972153), China Post-doctoral Science Foundation (2022M712582), and Shandong Natural Science Foundation (ZR2022QE037).

Declaration of competing interest

The authors have no competing interests to declare that are relevant to the content of this article. The author Weimin LIU is the Editorial Board Member of this journal.

Electronic Supplementary Material Supplementary material is available in the online version of this article at https://doi.org/10.1007/s40544-022-0714-6.

References

[1] Yan X, Yang B, Chen Y R, Song Y F, Ye J, Pan Y F, Zhou B N, Wang Y Q, Mao F B, Dong Y C, et al. Anti-friction MSCs delivery system improves the therapy for severe osteoarthritis. *Adv Mater* **33**(52): 2104758 (2021)

[2] Xie R, Yao H, Mao A S, Zhu Y, Qi D, Jia Y, Gao M, Chen Y, Wang L, Wang D A, et al. Biomimetic cartilage-lubricating polymers regenerate cartilage in rats with early osteoarthritis. *Nat Biomed Eng* **5**(10): 1189–1201 (2021)

[3] Lei Y T, Wang Y D, Shen J L, Cai Z W, Zhao C, Chen H, Luo X J, Hu N, Cui W G, Huang W. Injectable hydrogel microspheres with self-renewable hydration layers alleviate osteoarthritis. *Sci Adv* **8**(5): eabl6449 (2022)

[4] Rahimi M, Charmi G, Matyjaszewski K, Banquy X, Pietrasik J. Recent developments in natural and synthetic polymeric drug delivery systems used for the treatment of osteoarthritis. *Acta Biomater* **123**: 31–50 (2021)

[5] Bryk M, Chwastek J, Mlost J, Kostrzewa M, Starowicz K. Sodium monoiodoacetate dose-dependent changes in matrix metalloproteinases and inflammatory components as prognostic factors for the progression of osteoarthritis. *Front Pharmacol* **12**: 643605 (2021)

[6] Zhao B S, Li Y P, Wang Q N, Ren Y, Zheng Z L, Bai M H, Lv J C, Li K, Xu J Z, Li Z M, et al. Ultra-slippery, nonirritating, and anti-inflammatory hyaluronic acid-based coating to mitigate intubation injury. *Chem Eng J* **427**: 130911 (2022)

[7] Felson D T. Osteoarthritis: Virtual joint replacement as an outcome measure in OA. *Nat Rev Rheumatol* **8**(4): 187–188 (2012)

[8] Wan L, Wang Y, Tan X L, Sun Y L, Luo J, Zhang H Y. Biodegradable lubricating mesoporous silica nanoparticles for osteoarthritis therapy. *Friction* **10**(1): 68–79 (2022)

[9] Zhang W, Ouyang H W, Dass C R, Xu J K. Current research on pharmacologic and regenerative therapies for osteoarthritis. *Bone Res* **4**: 15040 (2016)

[10] Lin X J, Tsao C T, Kyomoto M, Zhang M Q. Injectable natural polymer hydrogels for treatment of knee osteoarthritis. *Adv Healthc Mater* **11**(9): e2101479 (2022)

[11] Feng W, Long P, Feng Y Y, Li Y. Two-dimensional fluorinated graphene: Synthesis, structures, properties and applications. *Adv Sci* **3**(7): 1500413 (2016)

[12] Kansara V, Shukla R, Flora S J S, Bahadur P, Tiwari S. Graphene quantum dots: Synthesis, optical properties and navigational applications against cancer. *Mater Today Commun* **31**: 103359 (2022)

[13] Wang Z D, Hu T T, Liang R Z, Wei M. Application of zero-dimensional nanomaterials in biosensing. *Front Chem* **8**: 320 (2020)

[14] Cardoso V F, Correia D M, Ribeiro C, Fernandes M M, Lanceros-Méndez S. Fluorinated polymers as smart materials for advanced biomedical applications. *Polymers* **10**(2): 161 (2018)

[15] Yu M N, Liu M M, Zhang D D, Fu S H. Lubricant-grafted omniphobic surfaces with anti-biofouling and drag-reduction performances constructed by reactive organic–inorganic hybrid microspheres. *Chem Eng J* **422**: 130113 (2021)

[16] Wang L, Gong P W, Li W, Luo T, Cao B Q. Mono-dispersed Ag/graphene nanocomposite as lubricant additive to reduce friction and wear. *Tribol Int* **146**: 106228 (2020)

[17] Tian R, Jia X H, Yang J, Li Y, Song H J. Large-scale, green, and high-efficiency exfoliation and noncovalent

functionalization of fluorinated graphene by ionic liquid crystal. *Chem Eng J* **395**: 125104 (2020)

[18] Tang W W, Zhang Z, Li Y F. Applications of carbon quantum dots in lubricant additives: A review. *J Mater Sci* **56**(21): 12061–12092 (2021)

[19] He C, E S, Yan H H, Li X J. Structural engineering design of carbon dots for lubrication. *Chinese Chem Lett* **32**(9): 2693–2714 (2021)

[20] Chung S, Revia R A, Zhang M Q. Graphene quantum dots and their applications in bioimaging, biosensing, and therapy. *Adv Mater* **33**(22): e1904362 (2021)

[21] Gong P W, Zhao Q, Dai D J, Zhang S M, Tian Z Z, Sun L, Ren J S, Liu Z. Functionalized ultrasmall fluorinated graphene with high NIR absorbance for controlled delivery of mixed anticancer drugs. *Chemistry* **23**(69): 17531–17541 (2017)

[22] Gong P W, Wang J Q, Hou K M, Yang Z G, Wang Z F, Liu Z, Han X X, Yang S R. Small but strong: The influence of fluorine atoms on formation and performance of graphene quantum dots using a gradient F-sacrifice strategy. *Carbon* **112**: 63–71 (2017)

[23] Ettefaghi E, Rashidi A, Ghobadian B, Najafi G, Ghasemy E, Khoshtaghaza M H, Delavarizadeh S, Mazlan M. Bio-nano emulsion fuel based on graphene quantum dot nanoparticles for reducing energy consumption and pollutants emission. *Energy* **218**: 119551 (2021)

[24] Gong J, Zhang Z Y, Zeng Z P, Wang W J, Kong L X, Liu J Y, Chen P. Graphene quantum dots assisted exfoliation of atomically-thin 2D materials and as-formed 0D/2D van der Waals heterojunction for HER. *Carbon* **184**: 554–561 (2021)

[25] Song S H, Wang D D, Zhao K, Wu Y T, Zhang P, Liu J F, Yang G, Gong P W, Liu Z. Donor–acceptor structured photothermal COFs for enhanced starvation therapy. *Chem Eng J* **442**: 135963 (2022)

[26] Yousaf M, Huang H, Li P, Wang C, Yang Y L. Fluorine functionalized graphene quantum dots as inhibitor against hIAPP amyloid aggregation. *ACS Chem Neurosci* **8**(6): 1368–1377 (2017)

[27] Chua C K, Sofer Z, Šimek P, Jankovský O, Klímová K, Bakardjieva S, Hrdličková Kučková Š, Pumera M. Synthesis of strongly fluorescent graphene quantum dots by cage-opening buckminsterfullerene. *ACS Nano* **9**(3): 2548–2555 (2015)

[28] Yang L K, Li Y W, Wang L Y, Pei Y X, Wang Z Y, Zhang Y, Lin H, Li X. Exfoliated fluorographene quantum dots as outstanding passivants for improved flexible perovskite solar cells. *ACS Appl Mater Inter* **12**(20): 22992–23001 (2020)

[29] Gong P W, Wang Z F, Wang J Q, Wang H G, Li Z P, Fan Z J, Xu Y, Han X X, Yang S R. One-pot sonochemical preparation of fluorographene and selective tuning of its fluorine coverage. *J Mater Chem* **22**(33): 16950–16956 (2012)

[30] Mathkar A, Narayanan T N, Alemany L B, Cox P, Nguyen P, Gao G H, Chang P, Romero-Aburto R, Mani S A, Ajayan P M. Synthesis of fluorinated graphene oxide and its amphiphobic properties. *Part Part Syst Char* **30**(3): 266–272 (2013)

[31] Yan Y F, Sun T, Zhang H B, Ji X L, Sun Y L, Zhao X, Deng L F, Qi J, Cui W G, Santos H A, et al. *Euryale Ferox* seed-inspired superlubricated nanoparticles for treatment of osteoarthritis. *Adv Funct Mater* **29**(4): 1807559 (2019)

[32] Zhang J Y, Zhou R H, Tang D D, Hou X D, Wu P. Optically-active nanocrystals for inner filter effect-based fluorescence sensing: Achieving better spectral overlap. *Trac-Trend Anal Chem* **110**: 183–190 (2019)

[33] Peng J Y, Gong P W, Li S H, Kong F, Ge X X, Wang B, Guo L H, Liu Z, You J M. A smart bioresponsive nanosystem with dual-modal imaging for drug visual loading and targeted delivery. *Chem Eng J* **391**: 123619 (2020)

[34] Chen S, Yu Y L, Wang J H. Inner filter effect-based fluorescent sensing systems: A review. *Anal Chim Acta* **999**: 13–26 (2018)

[35] Lin M, Zou H Y, Yang T, Liu Z X, Liu H, Huang C Z. An inner filter effect based sensor of tetracycline hydrochloride as developed by loading photoluminescent carbon nanodots in the electrospun nanofibers. *Nanoscale* **8**(5): 2999–3007 (2016)

[36] Gong P W, Zhao K, Liu X C, Li C, Liu B, Hu L Y, Shen D Y, Wang D D, Liu Z. Fluorescent COFs with a highly conjugated structure for combined starvation and gas therapy. *ACS Appl Mater Inter* **14**(41): 46201–46211 (2022)

[37] Shin K R, Kim Y S, Kim G W, Ko Y G, Shin D H. Development of titanium oxide layer containing nanocrystalline zirconia particles with tetragonal structure: Structural and biological characteristics. *Colloid Surface B* **131**: 47–53 (2015)

[38] Wu W, Liu J X, Gong P W, Li Z H, Ke C, Qian Y, Luo H W, Xiao L S, Zhou F, Liu W M. Construction of core–shell nanoMOFs@microgel for aqueous lubrication and thermal-responsive drug release. *Small* **18**(28): 2202510 (2022)

[39] Kong S, Wang J B, Hu W J, Li J S. Effects of thickness and particle size on tribological properties of graphene as lubricant additive. *Tribol Lett* **68**(4): 112 (2020)

[40] Mou Z H, Yang Q B, Zhao B, Li X Q, Xu Y X, Gao T T, Zheng H, Zhou K, Xiao D. Scalable and sustainable synthesis of carbon dots from biomass as efficient friction modifiers for polyethylene glycol synthetic oil. *ACS Sustain Chem Eng* **9**(44): 14997–15007 (2021)

[41] Ren K X, Yu G M, Zhang Z X, Wu W C, Tian P, Chhattal M, Gong Z B, Li Y, Zhang J Y. Self-organized transfer film-induced ultralow friction of graphene/$MoWS_4$

heterostructure nanocomposite. *Appl Surf Sci* **572**: 151443 (2022)

[42] Tang G B, Su F H, Xu X, Chu P K. 2D black phosphorus dotted with silver nanoparticles: An excellent lubricant additive for tribological applications. *Chem Eng J* **392**: 123631 (2020)

[43] Ji X L, Yan Y F, Sun T, Zhang Q, Wang Y X, Zhang M, Zhang H Y, Zhao X. Glucosamine sulphate-loaded distearoyl phosphocholine liposomes for osteoarthritis treatment: Combination of sustained drug release and improved lubrication. *Biomater Sci* **7**(7): 2716–2728 (2019)

[44] Chen H, Sun T, Yan Y F, Ji X L, Sun Y L, Zhao X, Qi J, Cui W G, Deng L F, Zhang H Y. Cartilage matrix-inspired biomimetic superlubricated nanospheres for treatment of osteoarthritis. *Biomaterials* **242**: 119931 (2020)

[45] Ahmed M R, Mehmood A, Bhatti F U R, Khan S N, Riazuddin S. Combination of ADMSCs and chondrocytes reduces hypertrophy and improves the functional properties of osteoarthritic cartilage. *Osteoarthr Cartilage* **22**(11): 1894–1901 (2014)

[46] Zhang K, Yang J L, Sun Y L, Wang Y, Liang J, Luo J, Cui W G, Deng L F, Xu X Y, Wang B, et al. Gelatin-based composite hydrogels with biomimetic lubrication and sustained drug release. *Friction* **10**(2): 232–246 (2022)

Peiwei GONG. He received his Ph.D. degree in 2015 from State Key Laboratory of Solid Lubrication, Lanzhou Institute of Chemical Physics (LICP), Chinese Academy of Sciences (CAS), China. He performed his postdoctoral research at Northwestern Polytechnical University, China, since 2020. Currently, He is an associate professor at Qufu Normal University, China. He has authored or co-authored more than 60 journal papers. His research interests focus on biotribology, solid lubrication, and tribochemistry.

Changmin QI. She received her B.S. degree in 2022 from Qufu Normal University, China. She is currently a Ph.D. student in LICP, CAS, China. Her research interests are biotribology and supramolecular gel lubricants.

Dandan WANG. She received her M.S. degree in 2013 from Changzhou University, China, and then worked as a research assistant in State Key Laboratory of Solid Lubrication, LICP, CAS, China. Presently, she is a lecturer of Qufu Normal University, China. Her research interests are biotribology, lubricating oil, and additives.

Mianran CHAO. She received her Ph.D. degree in 2015 from State Key Laboratory of Solid Lubrication, LICP, CAS, China. She is currently a lecturer in Qufu Normal University, China. She has authored or co-authored more than 15 journal and conference papers. Her research interests are lubricant additives, antioxidants, kinetics, and mechanism of oxidation reactions.

Jianxi LIU. He obtained his Ph.D. degree from Karlsruhe Institute of Technology, Germany, in 2015. He performed his postdoctoral research at Northwestern University, USA, from 2016 to 2018. In 2018, he started his independent research career at Northwestern Polytechnical University, China. Currently, He is an associate professor in Northwestern Polytechnical University, China. His research interests focus on smart lubrication, multifunctional coatings, nanofabrication, and optical sensing.

Meirong CAI. She obtained her Ph.D. degree in 2012 at LICP, CAS, China. She is currently a full professor at State Key Laboratory of Solid Lubrication, LICP, CAS, China. She has authored or co-authored 80 journal papers, which have received more than 1,500 citations and have the high-index of 24. Her research interests are tribochemistry, ionic liquid lubricants, and supramolecular gel lubricants.

Weimin LIU. He received his Ph.D. degree in lubricating materials and tribology from LICP, CAS, China, in 1990. Subsequently, he joined State Key Laboratory of Solid Lubrication, LICP, CAS, China. From June 1993 to June 1994, he worked as a visiting scholar at The Pennsylvania State University, USA. In 2013, he was elected a member of CAS, China. Currently, he is a professor of LICP, CAS, China. To date, he has published more than 500 papers with citations of over 39,000. He holds more than 100 Chinese patents and 1 U.S. patent and won 2 National Awards for Technological Invention (second class) and 2 National Awards for Natural Sciences (second class). He serves as one of the three chief editors of *Tribology International*. Currently, his research interests mainly focus on space and aviation lubrication, high-performance lubricating materials, and tribochemistry.